Science in China Series E: Technological Sciences

www.scichina.com
tech.scichina.com
www.springerlink.com

Post-earthquake assessment of building damage degree using LiDAR data and imagery

LI ManChun[1], CHENG Liang[1,2†], GONG JianYa[2], LIU YongXue[1], CHEN ZhenJie[1], LI FeiXue[1], CHEN Gang[1], CHEN Dong[1] & SONG XiaoGang[3]

[1] Department of Geographic Information Science, Nanjing University, Nanjing 210093, China;
[2] State Key Laboratory of Information Engineering in Surveying, Mapping and Remote Sensing, Wuhan University, Wuhan 430079, China;
[3] State Key Laboratory of Earthquake Dynamics, Institute of Geology, China Earthquake Administration, Beijing 100029, China

Various methods have been developed to detect and assess building's damages due to earthquakes using remotely sensed data. After the launch of the high resolution sensors such as IKONOS and QuickBird, it becomes realistic to identify damages on the scale of individual building. However the low accuracy of the results has often led to the use of visual interpretation techniques. Moreover, it is very difficult to estimate the degree of building damage (e.g. slight damage, moderate damage, or severe damage) in detail using the existing methods. Therefore, a novel approach integrating LiDAR data and high resolution optical imagery is proposed for evaluating building damage degree quantitatively. The approach consists of two steps: 3D building model reconstruction and rooftop patch-oriented 3D change detection. Firstly, a method is proposed for automatically reconstructing 3D building models with precise geometric position and fine details, using pre-earthquake LiDAR data and high resolution imagery. Secondly, focusing on each rooftop patch of the 3D building models, the pre- and post-earthquake LiDAR points belonging to the patch are collected and compared to detect whether it was destroyed or not, and then the degree of building damage can be identified based on the ratio of the destroyed rooftop patches to all rooftop patches. The novelty of the proposed approach is to detect damages on the scale of building's rooftop patch and realize quantitative estimation of building damage degree.

post-earthquake assessment, building damage degree, rooftop patch, LiDAR, imagery

Received December 19, 2008; accepted December 31, 2008
doi: 10.1007/s11431-008-6014-1
†Corresponding author (email: lcheng.geo@gmail.com)
Supported by the National Natural Science Foundation of China (Grant No. 40701117), Research Foundation for the Doctoral Program of Higher Education of China (Grant No. 20070284001), the National Basic Research Program of China ("973" Program) (Grant No. 2006CB701300), Foundation for University Key Teacher by the Chinese Ministry of Education, and the "985" Project of Nanjing University

1 Introduction

For decades, remote sensing techniques have been playing an important role in seismic disaster evaluation. Various methods have been developed to identify and assess building's damages using different resolutions satellite data. Many researches have been carried out after several recent big earthquakes such as the 1992 California Earthquake of USA[1—3], the 1995 Kobe Earthquake of Japan[4], the 1999 Kocaeli Earthquake of Turkey[5,6,7], the 2001 Gujarat Earthquake of India[8], and the 2003 Bam Earthquake of Iran[5,9,10].

Many researches are focused on developing damage assessment methods only using post-earthquake data, because the pre-earthquake satellite images may not always be available, and archived data with clear and suitable images is limited. Both visual and automated interpretations are used to derive the damage information from remotely sensed images. Saito et al. developed a damage assessment method only using a post-earthquake with high resolution satellite image[7]. An efficient automated methodology that detects damage was implemented to derive the rich information available from very high resolution satellite imagery[9]. Kohiyama and Yamazaki proposed an image fluctuation model method using middle-resolution satellite images, which employs a stochastic model of the digital number (*DN*) fluctuation in a normal condition[11]. Miura and Midorikawa updated the building inventory data by detecting the locations of newly constructed mid- and high-rise buildings from high-resolution satellite images and conducted a building damage assessment for a scenario earthquake using the updated inventory data[12]. Kaya et al. proposed a method of post-earthquake building collapse estimation from SPOT HRVIR data and identified that the result was very similar to government statistics[13]. Wang et al. introduced the study results in remotely sensed image fusion for identifying earthquake-caused building harm with HIS transform and intensity modulation[14].

In general, the change detection-based method, which compares pre- and post-earthquake images, can lead to more accurate and reliable results. Many studies on image matching were presented[15,16], which is the basis of change detection. Change detection capabilities of different features extracted from optical and radar data were compared and the potential of combining measurements at different frequency ranges was analyzed[5]. Turker and San used SPOT HRV (XS and PAN) images to detect earthquake-induced changes, the change areas were detected by subtracting the image brightness values for the near-infrared channel of the merged pre- and post-image and the overall accuracy of the change image was found to be 83%[17]. Matsuoka and Yamazaki performed a feasible study on backscattering characteristics of the damaged areas using the pre- and post-earthquake ERS images, revealing that the backscattering coefficient and intensity correlation between the two attained values were significantly lowered in hard-hit areas[18]. The suggestions on the use of proper satellite imagery were given by considering the area to cover, sensor type, spatial resolution, satellite's retake time, and etc.[19].

The availability of high resolution images allows the interpretation of damage scale of each building block or even each individual building; however it is very difficult to estimate the degree of building damage (e.g. slight damage, moderate damage, or severe damage) in detail using the existing methods. Therefore, a novel approach integrating LiDAR data and high resolution optical imagery is proposed for estimating building damage degree quantitatively. The approach consists of two steps: 3D building model reconstruction and rooftop patch-oriented 3D change detection. Firstly, a method is proposed for automatically reconstructing 3D building models with precise

geometric position and details, using pre-earthquake LiDAR data and high resolution imagery. Secondly, focusing on each rooftop patch of the 3D building models, the pre- and post-earthquake LiDAR points belonging to the patch are collected and compared to detect whether it was destroyed or not, and then the degree of building damage can be identified based on the ratio of the damaged rooftop patches to all rooftop patches.

2 3D building model reconstruction

2.1 Building boundary extraction

The extraction of building boundaries is a crucial and difficult step in generating building models. Before building boundary extraction, the LiDAR data need to be processed. During the LiDAR data processing, the ground points are separated from non-ground points firstly, and then the building points are identified from non-ground points, finally the segmented building points are obtained from raw LiDAR data. The algorithm proposed by Cheng and Gong[20] is used here, which can provide building boundaries with fine details and highly accurate geometric position, which is very important for the subsequent 3D building model reconstruction.

2.2 3D building boundary determination

After the boundary boundaries are extracted, the line-based photogrammetric intersection is often used to determine the 3D building boundaries. The main disadvantage of the method is that the accuracy of the determined 3D boundaries is largely influenced by the angle of interpretation plane and is lower than the accuracy of LiDAR data in the vertical direction. Therefore, a method is introduced for 3D boundary determination, which benefits to get 3D boundary segments with higher accuracy.

2.2.1 Intersecting ray with plane at *Z*. In order to overlap the extracted building boundary segments and LiDAR data, LiDAR points are directly projected onto the aerial images by means of the collinearity equation. Focusing on one endpoint of boundary segments, collect the LiDAR points around it and detect the edge points (the points on the building edges) among these points by Jiang et al.[21], then find the edge point nearest it. The height value of the nearest edge point is the height value of the endpoint. Since the height value of the endpoint has been obtained, three-dimensional coordinates of the point can be determined by intersecting a ray through the endpoint and the projection center with plane at the height value *Z*. The detailed calculation method is as follows, which is finally defined as formula (1).

$$\begin{bmatrix} x - x_0 \\ y - y_0 \\ -f \end{bmatrix} = \lambda \boldsymbol{M} \begin{bmatrix} X - X_{\mathrm{L}} \\ Y - Y_{\mathrm{L}} \\ Z - Z_{\mathrm{L}} \end{bmatrix},$$

where x and y are the coordinates of an image point; x_0 and y_0 are the coordinates of the image principal point; f is the focal length of the camera; X, Y and Z are the ground coordinates in ground space coordinate system; λ is the projection coefficient; $\boldsymbol{M}$ is the rotation matrix, which is defined as follows:

$$\boldsymbol{M} = \boldsymbol{M}_K \boldsymbol{M}_\phi \boldsymbol{M}_w,\ \boldsymbol{M}_w = \begin{bmatrix} 1 & 0 & 0 \\ 0 & \cos w & \sin w \\ 0 & -\sin w & \cos w \end{bmatrix},\ \boldsymbol{M}_\phi = \begin{bmatrix} \cos\phi & 0 & -\sin\phi \\ 0 & 1 & 0 \\ \sin\phi & 0 & \cos\phi \end{bmatrix},$$

$$\boldsymbol{M}_k = \begin{bmatrix} \cos k & \sin k & 0 \\ -\sin k & \cos k & 0 \\ 0 & 0 & 1 \end{bmatrix},$$

$$\frac{1}{\lambda}\boldsymbol{M}^{\mathrm{T}}\begin{bmatrix} x-x_0 \\ y-y_0 \\ -f \end{bmatrix} = \begin{bmatrix} X-X_{\mathrm{L}} \\ Y-Y_{\mathrm{L}} \\ Z-Z_{\mathrm{L}} \end{bmatrix}, \begin{bmatrix} u \\ v \\ w \end{bmatrix} = \boldsymbol{M}^{\mathrm{T}}\begin{bmatrix} x-x_0 \\ y-y_0 \\ -f \end{bmatrix}.$$

Rearranging with known Z, we can get

$$\begin{cases} X = X_{\mathrm{L}} + (Z - Z_{\mathrm{L}})\left(\dfrac{u}{w}\right), \\ Y = Y_{\mathrm{L}} + (Z - Z_{\mathrm{L}})\left(\dfrac{v}{w}\right). \end{cases} \tag{1}$$

A building is covered by four aerial images, as shown in Figure 1(a). Based on the method above, each aerial image can provide a dataset of 3D boundary segments by integrating the extracted 2D boundary segments and LiDAR data. As shown in Figure 1(b), four datasets of 3D boundary segments are derived from the corresponding aerial image.

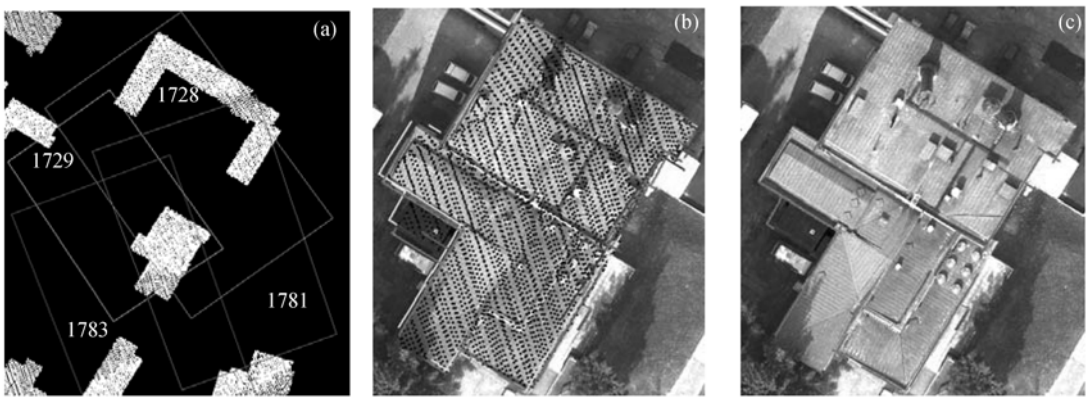

Figure 1 3D boundary determination. (a) A building covered by four aerial images; (b) four datasets of 3D boundary segments; (c) 3D boundary segments refinement.

2.2.2 3D boundary segment refinement. 3D boundary segments refinement becomes possible thanks to multi-view images. For example, as shown in Figure 1(b), four 3D segments are obtained for one real segment from four aerial images. The refinement processes include the following three steps.

Step 1: Grouping the segments. All the 3D segments are projected to the 2D X-Y plane. On the 2D plane, two segments are regarded as parallel if the angle between them is less than 4 degrees. All segments are grouped according to their angles and distances.

Step 2: Overlapping the segments and LiDAR data on the 2D plane. The segments with lower accuracy are removed by the algorithm based on LiDAR point density analysis and K-means clustering[22].

Step 3: RANSAC algorithm. Focusing on one group, RANSAC algorithm is used to construct a new segment according to all endpoints of the remaining segments. Comparing to least

squares method, RANSAC algorithm leads to the more robust results. Figure 1(c) shows the refinement results from Figure 1(b).

2.3 3D building rooftop line determination

For 3D rooftop line determination, the region-growing algorithm based on a plane-fitting technique proposed by Zhang et al.[23] is used to detect 3D rooftop patches. Given an inside point $p_0(x_0, y_0, z_0)$, a Cartesian coordinate system (x, y, z) is established using p_0 as the origin. In this coordinate system, a best fitting plane for p_0 and its eight neighbors are derived by using the least squares method. Assume that the plane is defined by

$$z = ax + by + c. \tag{2}$$

A plane is constructed based on the points in the category using a least squares fit. Considering that the segmented LiDAR points belong to a building (the white points in Figure 7), the region-growing processes are repeated to construct all rooftop planes. 3D rooftop line segments are determined based on intersection of the 3D rooftop planes.

2.4 An improved split-merge-shape method

In this section, an improved split-merge-shape method is proposed to recovery 3D building models from the determined 3D boundary segments and rooftop segments. To reconstruct 3D models using these 3D segments, the major problem is that the topology relationships between the segments are lost. The split-merge-shape method (SMS method) proposed by Rau and Chen[24] is an effective solution to automatically recover the topology relationships between these 3D segments. An improved SMS method based on LiDAR data is presented here. The main improvements cover the following two points. Firstly, the lost boundary segments can be automatically recovered. Secondly, the shaping process is finished by a more robust method.

The improved method includes four steps. 1) Separating the boundary segments from the rooftop segments using the boundary selection method proposed by Cheng[22]; 2) split-merge processes on boundary segments; 3) split-merge processes on rooftop segments; 4) shaping process. Splitting and merging processes are done on the 2D plane; shaping process is conducted in the 3D space. Regarding the split-merge processes on boundary segments, after the splitting process and before the merging process, the lost boundary recovery is conducted automatically.

2.4.1 Lost boundary recovery. As shown in Figure 2, the solid line segments are the discontinuous boundary segments. The outer rectangular box in Figure 2 is the initial building outline. Each solid segment is extended to split the outer box into two parts. Two boundaries never cross each other. Based on this truth, the solid segments should not cross each other, as shown in label B of Figure 2. Finally, many small regions surrounded by solid and dotted segments are created. The LiDAR point density of each small region can be calculated. In Figure 2, there are three types of polygon: polygons with small LiDAR density (label 1), polygons with large LiDAR density (label 2), and polygons with middle LiDAR density (label 3). If there are no lost boundary segments, only two types of polygon exist: one with large density and the other with small density. So we can identify that the lost boundary segments are located at the polygon of label 3 in Figure 2.

In this polygon, many rectangle boxes with a certain width (about 2 times the LiDAR point spacing) can be generated along the direction of one side, as shown in Figure 3(a). The LiDAR point density of these boxes can be calculated. The same processes are conducted along the perpendicular direction, as shown in Figure 3(b). The position in which the LiDAR point density

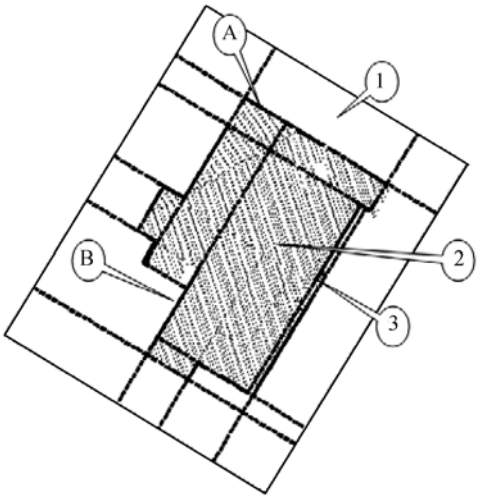

Figure 2 Split-merge processes on boundaries.

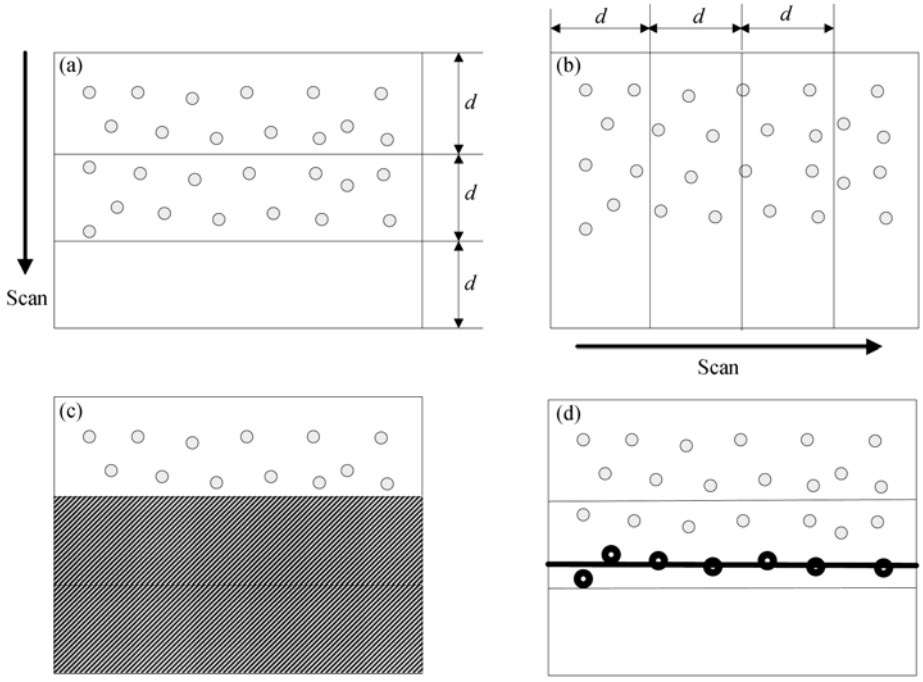

Figure 3 Scan detection. (a) Scan along one direction; (b) scan along the perpendicular direction; (c) the position of LIDAR density change; (d) edge points and the recovered segment.

largely is where the lost boundary should be located, as shown in Figure 3(c). The edge LiDAR points (bold points in Figure 3(d)) can be detected, and then a new segment can be constructed based on these points, which is the lost segment.

After the lost boundary segments are recovered, there are only two types of polygons: One with large LiDAR density and the other with small LiDAR density. The K-means clustering algorithm is employed here to divide a data set of LiDAR point density into two sets. All polygons with larger density are merged into a new large polygon. The outline of the new polygon is the complete

building boundary.

2.4.2 Robust shaping process. A complete boundary (Figure 4(b)) is derived from the discontinuous boundary segments (Figure 4(a)) by using the lost boundary recovery method above. Figure 4(c) consists of the complete building boundary and 3D rooftop lines. After recovering the topology between these lines using split-merge processes, many closed rooftop polygons are generated, shown in Figure 4(d). A 2D rooftop polygon can be reconstructed to a 3D patch by collecting and analyzing LiDAR points belonging to it. RANSAC algorithm is used here, because it can lead to more robust results than least squares method. As we know, there often exist many structures, such as water tower, funnel, and pipeline, on the top of building. In general, the LiDAR points on these top structures cannot be removed in the filtering processes. Due to these LiDAR points, the 3D rooftop patches reconstructed by least squares method have a low geometric accuracy in vertical direction. When reconstructing 3D models using RANSAC algorithm, these LiDAR points on the top restructures can be removed automatically, which will bring 3D models with higher accuracy, especially in vertical direction. Figure 4(e) shows the reconstructed 3D model.

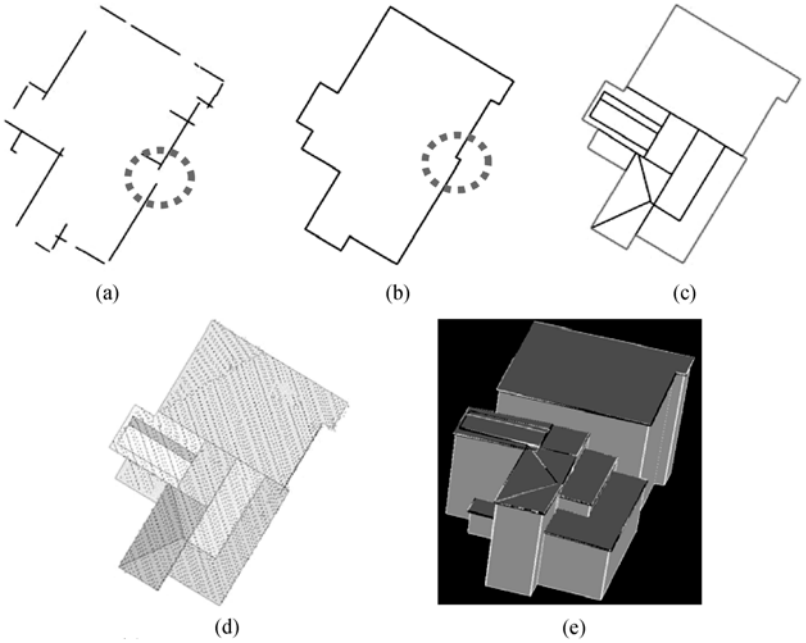

Figure 4 3D building model reconstruction. (a) 3D boundary segments; (b) a complete boundary; (c) the boundary and rooftop segments; (d) closed rooftop polygons and LiDAR points; (e) the constructed 3D model.

3 Rooftop patch-oriented 3D change detection

3.1 Rooftop patch destruction evaluation

Focusing on a rooftop patch of 3D building model, we can judge whether the rooftop patch has been destroyed or not, by collecting and comparing the pre- and post-earthquake LiDAR data belonging to it. All rooftop patches of building models are processed one by one. Each one can be identified as two types: undamaged or destroyed. As shown in Figure 5, the white plane means a rooftop patch of the building model in Figure 4(e). Figure 5 shows the pre- and post-earthquake LiDAR points, separately. The square sum of distance A can be calculated based on the pre-event

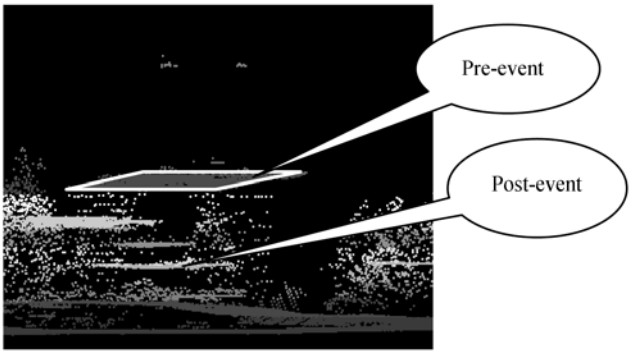

Figure 5 The destruction evaluation for a rooftop patch (white).

points and the plane. The square sum of distance B can also be calculated based on the post-event data and the plane. If B is about 4 times larger than A, the rooftop patch is identified as being destroyed; otherwise the rooftop patch is identified as being undamaged.

3.2 Building damage degree estimation

The estimation of building damage includes two parts: physical damage estimation, functional damage estimation. If evaluating the damage situation of building's physical structures in an earthquake, it is called physical damage estimation. Based on it, if further evaluating the bad influences on people's living and work caused by the building physical damages, it is called functional damage estimation. Focusing on building's physical damages, the paper establishes a scale of damage from 0 to 4, that is to say, the degree of building damage is divided into five grades. The five grades include no damage, slight damage, moderate damage, severe damage, and complete damage. In order to estimate the damage degree quantitatively, the concept of destroyed rooftop rate is used, which is defined as Formula (3). Table 1 shows the criteria for the gradation. Based on the rooftop patch destruction evaluation, every building can be graded according to its damage situation. All buildings can be estimated one by one, which is very useful for detailed assessment of earthquake-induced damage and post-earthquake reconstruction.

$$\text{Destroyed rooftop rate (\%)}=\frac{\text{Area of the destroyed rooftop patches}}{\text{Area of all rooftop patches}}. \tag{3}$$

Table 1 The degrees of building damage

Grade	Degree of damage	Criteria of estimation
0	No damage	No rooftop patches destroyed
1	Slight damage	Less than 30% rooftop patches destroyed
2	Moderate damage	30%—60% rooftop patches destroyed
3	Severe damage	60%—90% rooftop patches destroyed
4	Complete damage	More than 90% rooftop patches destroyed

4 Experiment and analysis

In this study, a local region of 365 m×415 m is chosen as the experimental region. Pre-event LiDAR data and pre-event multi-view aerial images are shown in Figures 6 and 7, respectively. Each aerial image is 3056×2032 pixels, with a spatial resolution of 5 cm, shown as a rectangle in Figure 7. The orientation parameters of the aerial stereo pair are known. LiDAR data in the same

area have average point spacing of 1.1 m. Figure 6 shows LiDAR points with different height values by different gray values. The white points in Figure 7 mean the segmented LiDAR data belonging to each building after pre-processing. The building damage assessment is conducted based on a scenario earthquake. In the scenario earthquake, different damage degrees of the different buildings are determined to be from 0 to 4 (0 = no damage; 4 = complete damage). The post-event LiDAR data are acquired by changing the height values of pre-event LiDAR data according to the damage status of each building after the scenario earthquake.

The experimental region covers 11 buildings, shown in Figure 7. Four buildings (01, 02, 07, and 11) cannot be reconstructed because the aerial images do not completely cover these buildings. Figure 8 shows the reconstructed 3D models of the other buildings. According to Figure 8, we can identify that the 3D models are reconstructed accurately by comparing the 3D models with the aerial images. With the support of the 3D models, the 3D change of each rooftop patch is detected by comparing the pre- and post-LiDAR data, which is to judge whether the rooftop was destroyed or not. As it is illustrated in Figure 9, the white polygons are the undamaged rooftop patches, the

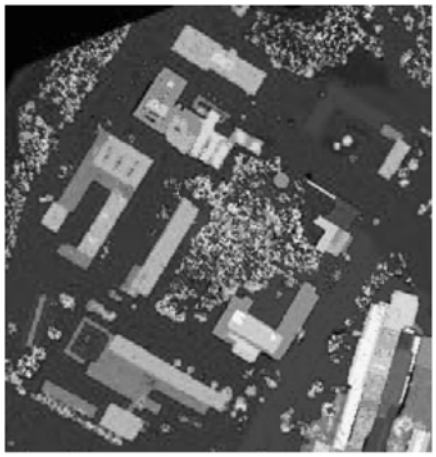

Figure 6 Pre-event LiDAR data.

Figure 7 Aerial images (rectangle box). White points: Segmented LiDAR data belonging to each building.

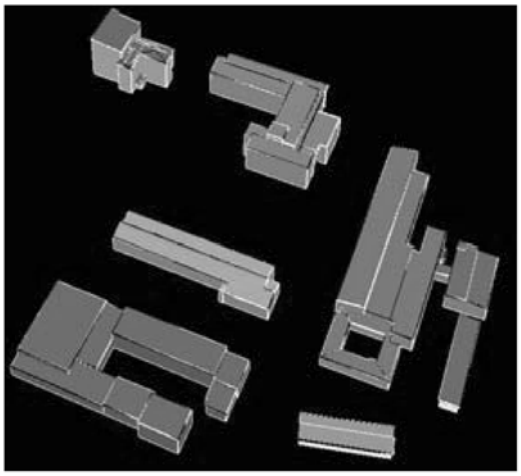

Figure 8 3D building models.

other black polygon are the destroyed rooftop patches. According to the damages of rooftop patches, the damage degree of the buildings can be identified. The detailed results are listed in Table 2. Figure 10 illustrates the damage degree of the buildings using different gray values.

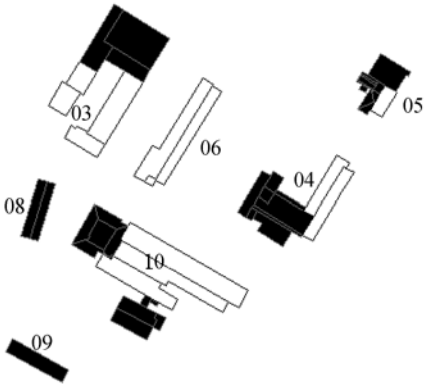

Figure 9 The damage status of rooftop patches (White: undamaged; black: Destroyed).

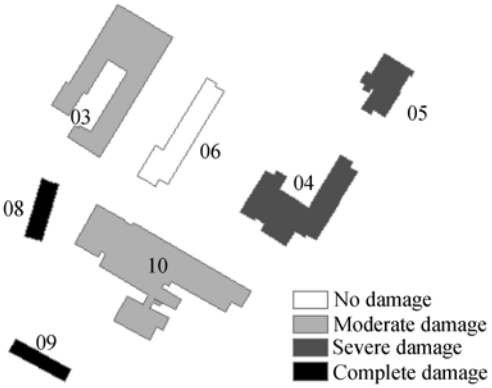

Figure 10 The damage degree of the buildings.

Table 2 The damage degree of the buildings

Building	Area of total rooftops	Area of destroyed rooftops	Destroyed rate	Damage degree
03	4127.01	2198.82	53%	Moderate damage
04	2744.2	2731.16	63%	Severe damage
05	1106.53	864.82	78%	Severe damage
06	1730.10	0	0%	No damage
08	619.92	619.92	100%	Complete damage
09	532.03	532.03	100%	Complete damage
10	5448.21	1895.07	35%	Moderate damage

5 Conclusion

A novel approach integrating LiDAR data and high resolution optical imagery is proposed for evaluating building damage degree quantitatively. The approach consists of two steps: 3D building model reconstruction and rooftop patch-oriented 3D change detection. Firstly, a method is proposed for automatically reconstructing 3D building models with precise geometric position and details, using pre-earthquake LiDAR data and high resolution imagery. Secondly, focusing on each rooftop patch of the 3D building models, the pre- and post-earthquake LiDAR data belonging to the patch are collected and compared to detect whether it was destroyed or not, and then the degree of building damage can be identified based on the ratio of the damaged rooftop patches to all rooftop patches. The novelty of the proposed approach is to detect damages on the scale of building's rooftop patch and realize building damage degree estimation quantitatively.

1 Massonnet D, Rossi M, Carmona C, et al. The displacement field of the Landers earthquake mapped by radar interferometry. Nature, 1993, 364(6433): 138－142
2 Blewitt G, Heflin M B, Hurst K J, et al. Absolute far-field displacements from the 28 June 1992 Landers earthquake sequence. Nature, 1993, 361(6410): 340－342
3 Bock Y, Agnew D C, Fang P, et al. Detection of crustal deformation from the Landers earthquake sequence using continuous geodetic measurements. Nature, 1993, 361(6410): 337－340
4 Matsuoka M, Yamazaki F. Characteristics of satellite images of damaged areas due to the 1995 Kobe earthquake. In: Proc

2nd Conf Appl Remote Sens GIS Disaster Manage. Washington: The George Washington University, 1999
5 Stramondo S, Bignami C, Chini M, et al. Satellite radar and optical remote sensing for earthquake damage detection: Results from different case studies. Int J Remote Sens, 2006, 27(20): 4433－4447
6 Estrada M, Matsuoka M, Yamazaki F. Use of Landsat images for the identification of damage due to the 1999 Kocaeli, Turkey earthquake. In: Proc 21st Asian Conf Remote Sens. Singapore, 2000. 1185－1190
7 Saito K, Spence R J S, Going C, et al., Using high-resolution satellite images for post-earthquake building damage assessment: A study following the 26 January 2001 Gujarat Earthquake. Earthq Spectra, 2004, 20(1): 145－169
8 Mitomi H, Yamazaki F, Matsuoka M. Automated detection of building damage due to recent earthquakes using aerial television images. In: Proc 21st Asian Conf Remote Sens. Singapore, 2000. 1185－1190
9 Vu T T, Matsuoka M, Yamazaki F. Detection and animation of damage using very high-resolution satellite data following the 2003 Bam, Iran, Earthquake. Earthquake Spectra, 2005, 21(S1): S319－S327
10 Yamazaki F, Yano Y, Matsuoka M, et al. Visual damage interpretation of buildings in bam city using QuickBird images following the 2003 Bam, Iran, Earthquake. Earthq Spectra, 2005, 21(S1): S329－S336
11 Kohiyama M, Yamazaki F. Image fluctuation model for damage detection using middle-resolution satellite imagery. Int J Remote Sens, 2005, 26(24): 5603－5627
12 Miura H, Midorikawa S. Updating GIS building inventory data using high-resolution satellite images for earthquake damage assessment: application to Metro Manila, Philippines. Earthq Spectra, 2006, 22(1): 151－168
13 Kaya S, Curran P J, Llewellyn G. Post-earthquake building collapse: A comparison of government statistics and estimates derived from SPOT HRVIR data. Int J Remote Sens, 2005, 26(13): 2731－2740
14 Wang H H, Du H, Chen M J, et al. Automatic identification of earthquake-caused building harm based on image fusion. In: Proc 2nd Int Conf Space Inform Technol. Bellingham: Society of Photo-Optical Instrumentation Engineers, 2007
15 Cheng L, Gong J, Yang X X, et al. Robust affine invariant feature extraction for image matching. IEEE Geosci Remote Sens Lett , 2008, 5(2): 246－250
16 Cheng L, Gong J, Song X G, et al. A method for affine invariant feature extraction with high quality for wide baseline stereo image matching (in Chinese). Acta Geodaetica et Cartographica Sinica, 2008, 37(1): 77－82
17 Turker M, San B T. SPOT HRV data analysis for detecting earthquake-induced changes in Izmit, Turkey. Int J Remote Sens, 2003, 24(12): 2439－2450
18 Matsuoka M, Yamazaki F. Use of satellite SAR intensity imagery for detecting building areas damaged due to earthquakes. Earthq Spectra, 2004, 20(3): 975－994
19 Yamazaki F, Matsuoka M. Remote sensing technologies in post-disaster damage assessment. J Earthq Tsunami, 2007, 1(3): 193－210
20 Cheng L, Gong J. Building boundary extraction using very high resolution images and LiDAR (in Chinese). Acta Geodaetica et Cartographica Sinica, 2008. 37(3): 91－93+99
21 Jiang J J, Zhang Z X, Ming, Y. Filtering of LiDAR point clouds for complex cityscapes (in Chinese). Geomatics Info Sci Wuhan Univ, 2007, 32(5): 402－405
22 Cheng L. 3D building model reconstruction from LiDAR data and Imagery (in Chinese). Dissertation of Doctoral Degree. Wuhan: Wuhan University, 2008
23 Zhang K, Yan J, Chen S. Automatic construction of building footprints from airborne LiDAR data. IEEE T Geosci Remote, 2006, 44(9): 2523－2533
24 Rau J Y, Chen L C. Robust reconstruction of building models from three-dimensional line segments. Photogramm Eng Rem S, 2003, 69(2): 181－188